Hindawi
Advances in Multimedia
Volume 2023, Article ID 9809705, 1 page
https://doi.org/10.1155/2023/9809705

Retraction

Retracted: Multimedia Detection and Processing of Remote-Sensing Image of Small Target Combined with Variable Neighborhood Search Algorithm

Advances in Multimedia

Received 15 August 2023; Accepted 15 August 2023; Published 16 August 2023

This article has been retracted by Hindawi following an investigation undertaken by the publisher [1]. This investigation has uncovered evidence of one or more of the following indicators of systematic manipulation of the publication process:

(1) Discrepancies in scope
(2) Discrepancies in the description of the research reported
(3) Discrepancies between the availability of data and the research described
(4) Inappropriate citations
(5) Incoherent, meaningless and/or irrelevant content included in the article
(6) Peer-review manipulation

The presence of these indicators undermines our confidence in the integrity of the article's content and we cannot, therefore, vouch for its reliability. Please note that this notice is intended solely to alert readers that the content of this article is unreliable. We have not investigated whether authors were aware of or involved in the systematic manipulation of the publication process.

Wiley and Hindawi regrets that the usual quality checks did not identify these issues before publication and have since put additional measures in place to safeguard research integrity.

We wish to credit our own Research Integrity and Research Publishing teams and anonymous and named external researchers and research integrity experts for contributing to this investigation.

The corresponding author, as the representative of all authors, has been given the opportunity to register their agreement or disagreement to this retraction. We have kept a record of any response received.

References

[1] Y. Wang and M. Qiu, "Multimedia Detection and Processing of Remote-Sensing Image of Small Target Combined with Variable Neighborhood Search Algorithm," *Advances in Multimedia*, vol. 2021, Article ID 9672749, 8 pages, 2021.

Hindawi
Advances in Multimedia
Volume 2021, Article ID 9672749, 8 pages
https://doi.org/10.1155/2021/9672749

Research Article

Multimedia Detection and Processing of Remote-Sensing Image of Small Target Combined with Variable Neighborhood Search Algorithm

Yaqin Wang[1] **and Maolong Qiu**[2]

[1]*School of Water Conservancy Engineering, Zhejiang Tongji Vocational College of Science and Technology, Hangzhou 311231, Zhejiang, China*
[2]*Zhejiang Qiantang River Administration Survey and Design Lnstitute, Hangzhou 310016, Zhejiang, China*

Correspondence should be addressed to Yaqin Wang; yxlm1985@st.btbu.edu.cn

Received 3 August 2021; Accepted 5 November 2021; Published 17 December 2021

Academic Editor: Zhendong Mu

The development of scientific satellites has made it a reality for people to view the Earth from the sky. However, due to the resolution of the image obtained, the effective and accurate interpretation of remote-sensing images has always been one of the goals pursued by the industry. In this paper, we merge the variable neighborhood search algorithm, reduce the accuracy of remote-sensing images, clean the invalid information of the data, use unsupervised classification methods to quickly locate small targets, use it as verification information, compare and select the image data through sample information, distinguish the background and target results, and get stable detection results. Practice shows that this method can effectively detect small targets in remote-sensing images.

1. Introduction

With the continuous increase in the number of perception images, remote sensing has become one of the important ways to understand the Earth. It uses satellites or drones to obtain spectral images of ground objects without touching objects and analyzes the spectral characteristics of the images and constantly recognizes features [1, 2]. The effective detection of image targets is to extract the probability feature distribution of different small targets from the image distribution results [3, 4]. Its application fields and directions are wide, such as urban optimization layout, target recognition and detection, and ecological environment monitoring [4, 5]. As one of the important ways of interpretation, it is extremely important to accurately and effectively identify the target and dig the target. Traditional detection methods can perform target detection through statistics, target detection through existing knowledge, and target detection through established models. All of these need to set priority conditions, and it is difficult to automate large-scale image interpretation [6–8].

For traditional remote-sensing image interpretation, it can be divided into supervised classification and unsupervised classification according to the interpretation method. Supervised classification is to first determine a certain sample and extract similar targets based on the sample, but the acquisition of the sample is subject to the comprehensive restrictions of image acquisition and spectrum acquisition, and the selection of samples also has certain restrictions. Therefore, how to select specific supervised classification results from effective image interpretation to meet the final classification requirements? unsupervised classification is to directly perform interpretation and classification without samples and obtain the final result [9, 10]. Although this method is simple and easy to implement, because there is no sample, there will often be missed judgments or misjudgments, which are a lot of work for the later stage [11, 12].

Therefore, in response to this problem, this paper integrates the variable neighborhood search algorithm to detect and process small multimedia targets in remote-sensing images, separate the target and background in space

according to the small targets, and distinguish the remote-sensing image multimedia detection and processing.

2. Multimedia Detection Method of Small Target Based on Hyperspectral Remote-Sensing Image

The small target multimedia detection of remote-sensing images is comprehensively analyzed through comprehensive unsupervised classification and support vector machines, and the adaptive feedback determination rules are clarified, including the dimensionality reduction of remote-sensing images, verification information extraction, adaptive adjustment and optimization, and small target multimedia detection and analysis; the specific flowchart is shown in Figure 1:

2.1. Dimensionality Reduction of Hyperspectral Remote-Sensing Images and Acquisition of Posterior Information. Although remote-sensing images can provide a wealth of spectral information, the spectra of adjacent ground objects have obvious respiratory relevance, which can easily lead to errors in the classification of adjacent maps and aggravate the increase in the magnitude of the map calculation and information. Therefore, it is necessary to eliminate redundant information and clarify the main extraction information. Therefore, based on the acquired images, this article performs principal component analysis calculations on the map information, maps high-dimensional data to low-dimensional data, and eliminates redundant and invalid information, which significantly reduces the amount of data and reduces the calculation. Data are based on principal component analysis to perform dimensionality reduction analysis on remote-sensing image data.

On this basis, the unsupervised classification method is used to locate small targets in remote-sensing images, which lays a verification foundation for accurate identification, reduces the workload of detection, and improves the efficiency of detection [13–15].

2.2. Adaptive Determination of SVM Kernel Function Parameters Based on the Kernel Space Divergence Criterion. In the process of small target detection, the most important thing is the spectral data detection of remote-sensing images. Based on the expanded nuclear space, this paper further clarifies that the parameters of the kernel function are optimized by the intraclass and interclass distance difference or distance ratio in the largest nuclear space and gives the corresponding fast iteration formula.

For $N_k(x)$ and EST_{im} between two pixels, the inner product in the kernel space can be indirectly calculated by the kernel function using the following formula:

$$\begin{aligned}\Phi\left(x_{t_i}\right)^T \cdot \Phi\left(x_{t_j}\right) &= \left\langle \Phi\left(x_{t_i}\right), \Phi\left(x_{t_j}\right) \right\rangle = \mathrm{Ker}\left(x_{t_i}, x_{t_j}\right) \\ &= K_{t_i t_j} = \exp\left(-\frac{1}{2e}\left\|x_{t_i} - x_{t_j}\right\|_2\right).\end{aligned} \tag{1}$$

The calculation formula for the central pixel LST_{im} of a certain type of pixel in the kernel space and the central pixel of all the pixels LST_{im} is shown in the following formula:

$$\begin{aligned}\overline{\Phi\left(x_t\right)} &= \frac{1}{N_t}\sum_{i=1}^{N_t}\Phi\left(x_{t_i}\right), \\ \overline{\Phi\left(x\right)} &= \frac{1}{N}\sum_{t=1}^{C}\sum_{i=1}^{N_t}\Phi\left(x_{t_i}\right).\end{aligned} \tag{2}$$

The calculation formula of the intraclass divergence L_m in the kernel space is shown in the following formula:

$$\begin{aligned}S_w &= \sum_{t=1}^{C}\left\{\frac{N_t}{N}\sum_{i=1}^{N_t}\frac{1}{N_t}\left\{\left[\Phi\left(x_{t_i}\right) - \overline{\Phi\left(x_t\right)}\right]^T \cdot \left[\Phi\left(x_{t_i}\right) - \overline{\Phi\left(x_t\right)}\right]\right\}\right\} = \\ &\sum_{t=1}^{C}\sum_{i=1}^{N_t}\left\{\frac{1}{N}\left[\Phi\left(x_{t_i}\right) - \frac{1}{N_t}\sum_{z=1}^{N_t}\Phi\left(x_{t_i}\right)\right]^T \cdot \left[\Phi\left(x_{t_i}\right) - \frac{1}{N_t}\sum_{z=1}^{N_t}\Phi\left(x_{t_i}\right)\right]\right\} = \\ &\frac{1}{N}\sum_{t=1}^{C}\sum_{z=1}^{N_t}\left[\Phi\left(x_{t_i}\right)^T\Phi\left(x_{t_i}\right) - \frac{1}{N_t}\sum_{z=1}^{N_t}\Phi\left(x_{t_i}\right)^T\Phi\left(x_{t_i}\right)\right. \\ &\left.-\frac{1}{N_t}\sum_{z=1}^{N_t}\Phi\left(x_{t_i}\right)^T\Phi\left(x_{t_i}\right) + \frac{1}{N_t^2}\sum_{z=1}^{N_t}\sum_{l=1}^{N_t}\Phi\left(x_{t_i}\right)^T\Phi\left(x_{t_i}\right)\right] = \\ &\frac{1}{N}\sum_{t=1}^{C}\sum_{i=1}^{N_t}\left(K_{t_i t_j} - \frac{1}{N_t}\sum_{i=1}^{N_t}K_{t_z t_i} - \frac{1}{N_t}\sum_{l=1}^{N_t}K_{t_i t_l} + \frac{1}{N_t^2}\sum_{z=1}^{N_t}\sum_{l=1}^{N_t}K_{t_z t_l}\right) = \frac{1}{N}\sum_{t=1}^{C}\sum_{i=1}^{N_t}\overline{K_{t_i t_i}}.\end{aligned} \tag{3}$$

Middle L_m represents the L_mth element of the centralizing kernel matrix within the class.

Analogous to the derivation method of S_w, the calculation formula of the interclass divergence S_b in the kernel space can be obtained as shown in the following formula:

$$\begin{aligned} S_b &= \sum_{t=1}^{C}\left\{\frac{N_t}{N}\sum_{i=1}^{N_t}\left\{\left[\overline{\Phi\left(x_{t_i}\right)}-\overline{\Phi(x)}\right]^T\cdot\left[\overline{\Phi\left(x_{t_i}\right)}-\overline{\Phi(x)}\right]\right\}\right\}\approx \\ &\frac{1}{N}\sum_{t=1}^{C}\sum_{i=1}^{N_t}\left\{\left[\Phi\left(x_{t_i}\right)-\overline{\Phi(x)}\right]^T\cdot\left[\Phi\left(x_{t_i}\right)-\overline{\Phi(x)}\right]\right\}= \\ &\frac{1}{N}\sum_{t=1}^{C}\sum_{i=1}^{N_t}\left[K_{t_it_j}-\frac{1}{N}\sum_{p=1}^{C}\sum_{z=1}^{N_p}K_{p_zt_i}-\frac{1}{N}\sum_{q=1}^{C}\sum_{z=1}^{N_q}\left(\sum_{q=1}^{C}\sum_{l=1}^{N_q}K_{p_zq_l}\right)\right]=\frac{1}{N}\sum_{t=1}^{C}\sum_{i=1}^{N_t}\left(\overline{K_{t_it_i}}\right)', \end{aligned} \tag{4}$$

where N_q is the total number of type q pixels, where $q = 1,2, \ldots, C$, and $\sum_{q=1}^{C} N_q = N$, N_q is the total number of type P pixels, where $p = 1, 2, \ldots, C$, $\sum_{p=1}^{C} N_p = N$, and $(\overline{K_{t_it_i}})'$ represents the (t_i, t_i)th element of the interclass centralized kernel matrix.

$MAP^{R_{IoU}=0.50}$ and $MAP^{R_{IoU}=0.50}$ can be calculated by the following formula:

$$\begin{cases} \nabla K_{t_it_j}=\exp\left(-\dfrac{1}{2e}\left\|x_{r_i}-x_{t_j}\right\|_2\right)\cdot\dfrac{1}{2e^2}\cdot\left\|x_{t_i}-x_{t_j}\right\|_2, \\ \overline{\nabla K_{t_it_i}}=\nabla K_{t_it_i}-\dfrac{1}{N}\sum_{z=1}^{N_t}\nabla K_{t_zt_i}-\dfrac{1}{N_t}\sum_{l=1}^{N_t}\nabla K_{t_it_l}+\dfrac{1}{N_t^2}\sum_{z=1}^{N_t}\sum_{l=1}^{N_t}\nabla K_{t_zy_l}, \\ \left(\overline{\nabla K_{t_it_l}}\right)'=\nabla K_{t_it_i}-\dfrac{1}{N}\sum_{p=1}^{C}\sum_{z=1}^{N_p}\nabla K_{p_zt_i}-\dfrac{1}{N}\sum_{q=1}^{C}\sum_{l=1}^{N_q}\nabla K_{t_iq_l}+\dfrac{1}{N^2}\sum_{p=1}^{C}\sum_{z=1}^{N_p}\left(\sum_{q=1}^{C}\sum_{l=1}^{N_q}\nabla K_{p_zq_l}\right), \\ \nabla S_1=\sum_{t=1}^{C}\sum_{i=1}^{N_t}\dfrac{1}{N}\cdot\left(\overline{\nabla K_{t_it_i}}\right)'-\sum_{t=1}^{C}\sum_{i=1}^{N_t}\dfrac{1}{N}\cdot\overline{\nabla K}_{t_it_i}, \\ \nabla S_2=\dfrac{S_w\cdot\left[\sum_{t=1}^{C}\sum_{i=1}^{N_t}1/N\cdot\left(\overline{\nabla K_{t_it_i}}\right)'\right]-S_b\cdot\left[\sum_{t=1}^{C}\sum_{i=1}^{N_t}1/N\cdot\overline{\nabla K}_{t_it_i}\right]}{S_w^2}. \end{cases} \tag{5}$$

Then, the iterative formula of the kernel parameter e is

$$e_{\text{update}} = e_{\text{before}} + \lambda\cdot\text{rand}\cdot\text{sign}(\nabla S)\cdot e_{\text{before}}. \tag{6}$$

Among them, the value range of rand is (0, 1), the symbolic function is MAP^{large}, and the iteration step size is represented by λ.

2.3. Algorithm Overall Flow. Aiming at the problem of small target detection, a multiobjective VNS (MOVNS) algorithm is designed to obtain the Pareto solution set of the problem. Let x be the current solution of the problem, $N_k(x)(k = 1, \ldots, k_{\max})$ be the adjacent solution set of x under the kth neighborhood structure, and P be the Pareto solution set maintained during the operation of the algorithm. The overall flow of the MOVNS algorithm is as follows:

Step 1: Generate the initial solution x, $P = (x)$, the maximum number of iterations maxIter, count = 0;

Step 2: While(count ≤ maxlter)

For $k = 1$ To $k_{\max}$;

Randomly select the solution % in P, randomly select the objective function $r \in \{1,2\}$ for optimization; perform a local search based on the neighborhood structure $N_k(x)$ to obtain the local optimal solution x′;

If x′ is Pareto Solution

Then P: =P∪{x′}; delete the solution dominated by x′ from P; count = 0; Else count++;

Step 3: Output Pareto solution set P.

The initial solution and neighborhood structure of the MOVNS algorithm are described in the previous two sections.

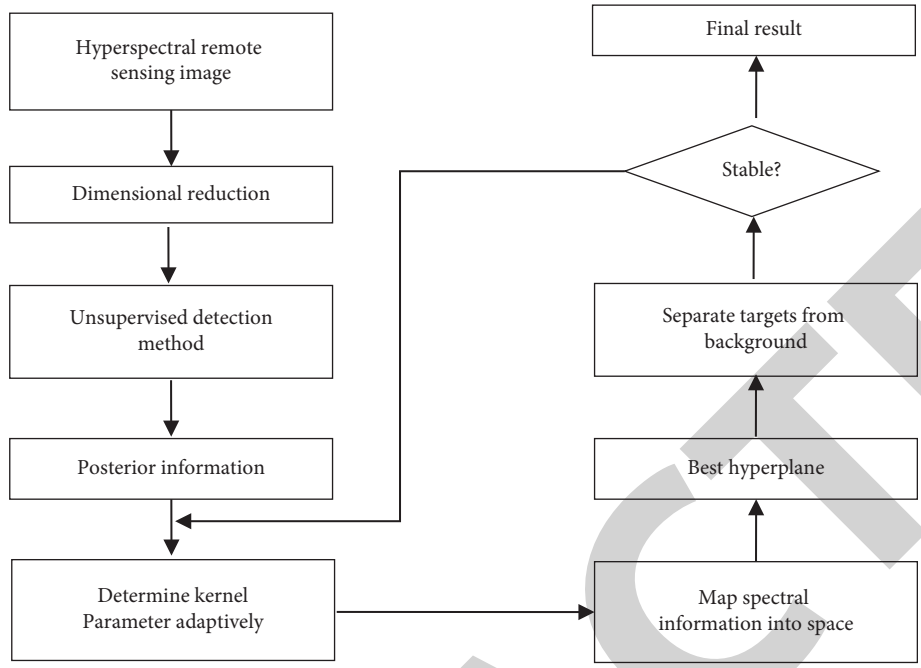

Figure 1: Flowchart of the small target detection method in hyperspectral remote-sensing image.

2.4. Initial Solution Generation Process. In the contract scheduling problem in this study, the manufacturing process of each work order has been determined, that is, the unit through which the process passes is known. Contract scheduling starts on the 1st day and ends on the ITI day. Using forward and reverse calculation methods, the earliest start time EST_{im} and the latest start time LST_{im} of each unit can be calculated for each work order. The initial solution generation process only considers the optimization objective (2), and the process is as follows.

Initial solution generation process:

Step 1: for the work orders to be processed on the unit $m \in M$, sort them in increasing order of LST_{im} to get the work order list L_m;

Step 2: for $t = 1$ To $|T|$

For $m = 1$ To $|M|$

According to the order of work orders in L_m and considering the capacity constraints of unit m, the work order is scheduled for production on day t of unit m. If the arrangement is successful, the work order will be deleted from L_m;

Step 3: output the initial solution.

2.5. Neighborhood Structure. In the search process, the VNS algorithm needs to alternately test new solutions in neighborhoods of different structures to improve the current solution. The MOVNS algorithm in this paper uses three neighborhood structures, namely, $N2(x)$ = Insertion neighborhood, $N2(x)$ = Swap neighborhood, and $N3(x) = 2$Insertion neighborhood.

The Insertion neighborhood search process deletes a work order from the current solution and reinserts it into other time periods in the solution to obtain a new solution. In the implementation process, due to the huge number of work orders, in order to save the running time of the algorithm, 400, 500, 600, 700, and 800 work orders were randomly selected for insertion neighborhood search instead of neighborhood search for all work orders.

The Swap neighborhood search process selects two work orders with the same process in turn and exchanges their processing time periods on each unit to obtain a new solution.

The Insertion neighborhood search process is similar to the Insertion neighborhood search process. The difference is that two adjacent work orders are selected and reinserted to the best position in the current solution to obtain a new solution.

The above neighborhood search operations are all performed under the premise of satisfying the constraints of the actual problem. Therefore, it is possible to search as many neighborhoods as possible, increase the probability of finding a better solution, and save the execution time of the algorithm.

3. Experimental Analysis

3.1. Experimental Platform and Data. In order to verify the performance of the variable neighborhood search algorithm in the multimedia detection of remote-sensing images of small targets, scale production of large, medium, and small targets based on related datasets, collect typical data sets such as airplanes and sports fields, and collect the work through

remote-sensing image targets, the test training sample is expanded. The sample data collected this time provide 2600 pieces, of which 440 pieces are used for verification datasets and 330 pieces are tested datasets. The target distribution of statistical samples is shown in Figure 2. With the division and collection of small targets, various datasets are distributed and identified based on small and medium targets.

In order to judge the validity and accuracy of the detection, an interactive comparison is made based on the existing dataset, and then, a judgment is made based on the built-in reliability of the prediction to detect the effectiveness of small target recognition.

In this study, first, according to the detection of hyperspectral multimedia small target detection method of variable neighborhood search algorithm, a large number of small target multimedia detection is carried out, and it is compared with the existing RX method (the first method) and the nuclear RX method (the second method). For comparison, the histogram segmentation method can be used to extract small targets for both the first method and the second method. The parameters are set according to the characteristics of the remote-sensing image. The method in this article is compared with the three comparison methods to ensure the superiority of the method and to verify the insensitivity of the method according to all the clarification of the detection error value.

Use the defined detection rate Pd and the false alarm rate Pf to quantitatively analyze the detection results. The specific calculation is shown in the following formula:

$$P_d = \frac{N_{\text{hit}}}{N_{\text{target}}}, \qquad P_f = \frac{N_{\text{false}}}{N_{\text{total}}}, \tag{7}$$

where N_{hit} is the number of detected real target pixels, N_{target} is the total number of real target pixels, the false alarm rate N_{false} is the number of false alarm pixels detected, and N_{total} is the total number of pixels in the entire image.

3.2. Training Analysis of Variable Neighborhood Search Algorithm. Data enhancement uses processes such as cropping, rotation, and scaling for attenuation analysis. The specific attenuation curve is shown in Figure 3:

Perform batch processing for the loss function. The specific training curve is shown in Figure 4. The final value of the loss can be controlled within the range of (0, 1), and the convergence effect is relatively good. The small target of the variable neighborhood search algorithm multimedia detection can effectively train, and the reverse is not easy to diverge, which verifies the effectiveness of the algorithm structure.

3.3. Accuracy Analysis of Variable Neighborhood Search Algorithm. In order to verify the performance of the variable neighborhood search algorithm, the training set was used to train Faster R-CNN and R-FCN based on the candidate box method as a comparison, and the accuracy verification was performed on the verification set. Faster R-CNN was used, respectively. Two networks, ResNet50 and ResNetlO1, are used as the basic network. R-FCN uses ResNetl01 as the basic network and uses the more accurate Inceptionv2 network to replace the VGG16 of the SSD algorithm. It also participates in the comparison experiment. The input size of the above algorithm image is 800pixll × 800 pixel. Except for the variable neighborhood search algorithm, the other algorithms all use the pretrained model on the COCO dataset for migration learning, and the variable neighborhood search algorithm uses the migration method mentioned above. Part of the parameter migration is performed. The above algorithms are trained and iterated 1.5×10^5 times, and the accuracy analysis and statistics are performed on the verification set and the test set, respectively. The comparison result of single image prediction time-consuming and verification set accuracy index is shown in Figure 5.

It can be seen from Figure 6 that the model parameters of the variable neighborhood search algorithm are only increased by 6.4 MB compared with SSD + Inceptionv2, but compared with Faster R-CNN and R–FCN algorithms, it is much lower, especially only 23% of R-FCN + ResNet101. From the perspective of predicting the time cost of a single image, the variable neighborhood search algorithm increases 47 ms compared with SSD + Inceptionv2, but decreases compared with Faster R-CNN and R-FCN algorithms, especially compared with Faster R-CNN + ResNet101. It decreases by 45.7 ms. From the perspective of accuracy indicators, the variable neighborhood search algorithm has a 1.38% reduction in the detection accuracy of large targets on the verification set, MAP^{large}, compared to R-FCN + ResNet101, and other indicators are better than other methods, especially in detecting small targets. In the test set, MAP^{small} increased by 13.92% compared with the second highest R-FCN + ResNet101, which shows that the variable neighborhood search algorithm has obvious advantages in detecting medium and small targets. It can be seen from the results that the Faster R–CNN and R–FCN algorithms converge faster than the variable neighborhood search algorithm, indicating that the improved SSD algorithm has a relatively long convergence time, which has a certain relationship with the random initialization of some of the parameters. The domain search algorithm and the SSD + Inceptionv2 algorithm show that the accuracy of SSD + Inceptionv2 fluctuates greatly with the number of iteration steps, especially the accuracy mutation of small targets is the most obvious. This shows that the SSD algorithm has a poor training effect on small target datasets, which is further verified. The low-level features of SSD are poor for small target recognition, but the variable neighborhood search algorithm can better adapt to the small target data, and the change of each accuracy index of the variable neighborhood search algorithm is generally relatively stable.

From the above calculation results, compared with the SSD algorithm, R-CNN algorithm, and R-FCN algorithm, the variable neighborhood search algorithm has more obvious advantages in small target detection; from the time-

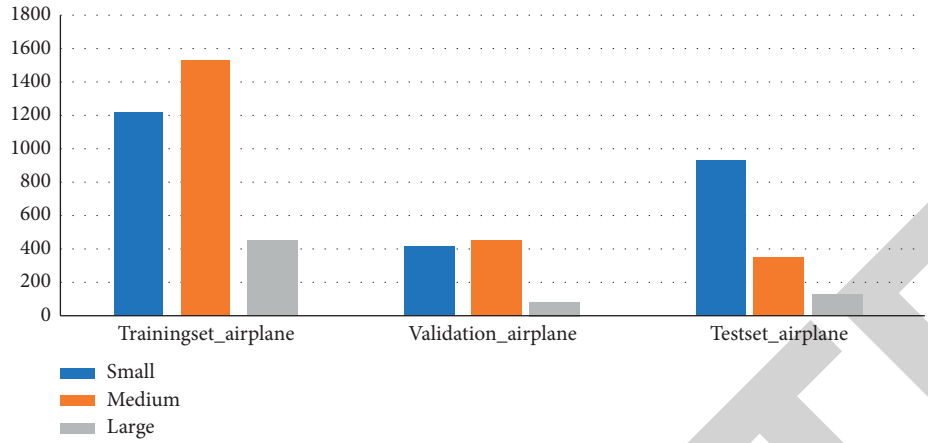

Figure 2: Sample set statistics.

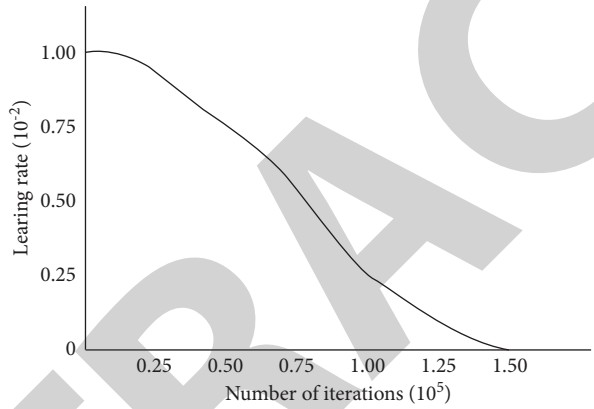

Figure 3: Learning rate decay curve.

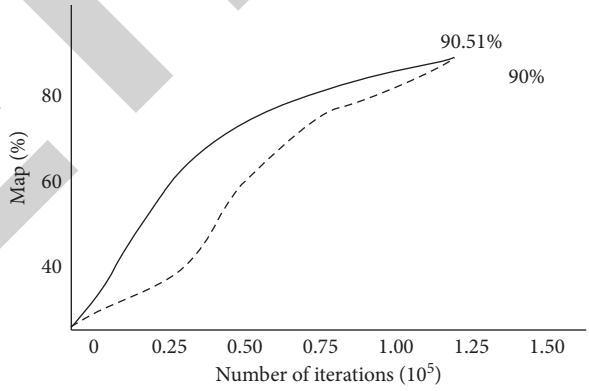

Figure 4: Comparison of total loss and accuracy of migration training and random initialization (varies with the number of iterations).

consuming point of view, the variable neighborhood search algorithm effectively reduces the time required, and at the same time, it can solve the problem of poor adaptation of the algorithm to small target sample datasets. Therefore, for the variable neighborhood search algorithm, its advantages are more obvious, the results are more accurate, and the efficiency is more efficient.

3.4. Comparison of Detection Results. According to the detection results, the main reason is the integrated detection. There is no process of preset samples. The variable neighborhood search algorithm can effectively predict small targets, and the verified information is not affected by the detection of unsupervised analysis. Compared to others, as far as the algorithm is concerned, the variable domain search

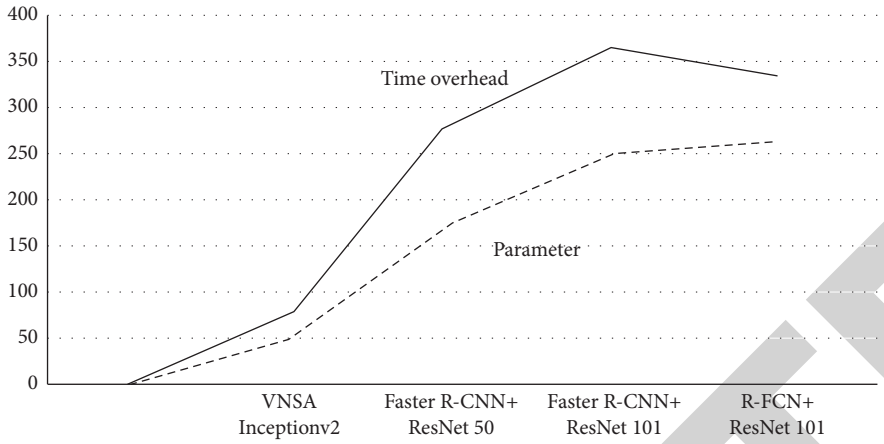

Figure 5: Comparison of calculation time and accuracy on the verification set.

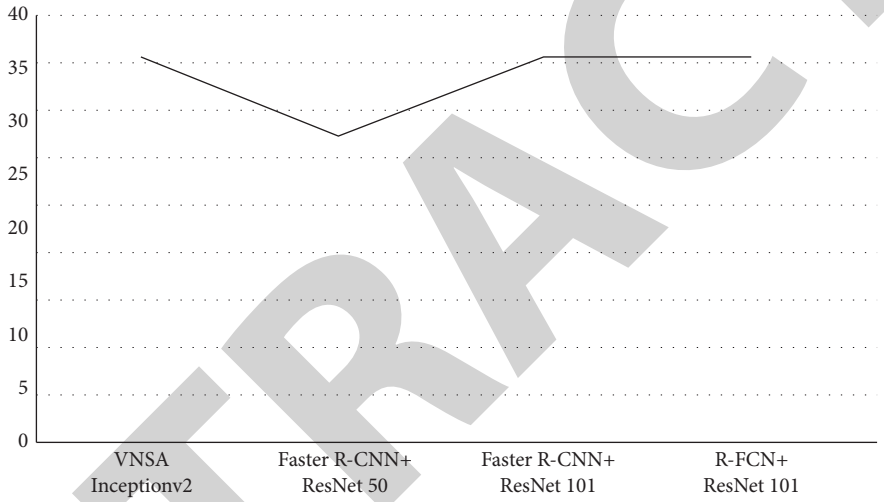

Figure 6: Accuracy comparison on the test set.

algorithm has obvious stability and effectiveness for iterative detection of small targets.

4. Conclusions

Remote-sensing image small target detection is one of the important remote-sensing image difficulties. In this paper, the variable domain search algorithm is integrated to detect small targets separately, using dimensionality reduction, unsupervised classification, adaptive determination, and support vector machine for small target detection. Practice results prove that the method is effective.

Data Availability

The data used to support the findings of this study are available from the corresponding author upon request.

Conflicts of Interest

The authors declare no conflicts of interest.

Acknowledgments

This research study was sponsored by Fundamental Scientific Research Business Fee Project for Universities in Zhejiang Province (project no. FRF21YB022).

References

[1] Z. Zou and Z. Shi, "Random access memories: a new paradigm for target detection in high resolution aerial remote sensing images," *IEEE Transactions on Image Processing*, vol. 2, no. 99, pp. 1–10, 2017.

[2] X. Wang, C. Ning, and L. Xu, "Spatiotemporal difference-of-Gaussians filters for robust infrared small target tracking in

various complex scenes," *Applied Optics*, vol. 54, no. 7, pp. 1573–1586, 2015.

[3] C. Lee, M. Han, and J. Baek, "SU-E-I-10: investigation on detectability of a small target for different slice direction of a volumetric cone beam CT image," *Medical Physics*, vol. 42, no. 6, p. 3243, 2015.

[4] M. Wan, G. Gu, W. Qian, K. Ren, and Q. Chen, "Robust infrared small target detection via non-negativity constraint-based sparse representation," *Applied Optics*, vol. 55, no. 27, pp. 7604–7612, 2016.

[5] C. Wang and S. Qin, "Adaptive detection method of infrared small target based on target-background separation via robust principal component analysis," *Infrared Physics & Technology*, vol. 69, no. 2, pp. 123–135, 2015.

[6] J. H. Ryu, H. S. Jung, and S. Lee, "Special issue on advances in remote sensing and geoscience information systems of the coastal environments," *Journal of Coastal Research*, vol. 90, no. 1, pp. 904–908, 2019.

[7] S. Kim, "Acoustic detection of small unmanned aerial system using mills cross arrays," *Journal of the Acoustical Society of America*, vol. 140, no. 4, p. 3120, 2016.

[8] A. W. Nolin, "Recent advances in remote sensing of seasonal snow," *Journal of Glaciology*, vol. 56, no. 200, pp. 1141–1150, 2017.

[9] Z. Cui, J. Yang, S. Jiang, and J. Li, "An infrared small target detection algorithm based on high-speed local contrast method," *Infrared Physics & Technology*, vol. 76, no. 5, pp. 474–481, 2016.

[10] J. Z. Kosicki, K. Stachura, M. Ostrowska, and E. Rybska, "Complex species distribution models of Goldcrests and Firecrests densities in Poland: are remote sensing-based predictors sufficient?" *Ecological Research*, vol. 30, no. 4, pp. 625–638, 2015.

[11] D. A. Neave, M. Black, T. R. Riley et al., "On the feasibility of imaging carbonatite-hosted rare earth element deposits using remote sensing," *Economic Geology*, vol. 111, no. 3, pp. 641–665, 2016.

[12] M. Nasiri, M. R. Mosavi, and S. Mirzakuchaki, "Infrared dim small target detection with high reliability using saliency map fusion," *IET Image Processing*, vol. 10, no. 7, pp. 524–533, 2016.

[13] J. Guo, Y. Wu, and Y. Dai, "Small target detection based on reweighted infrared patch-image model," *IET Image Processing*, vol. 12, no. 1, pp. 70–79, 2018.

[14] H. Qin, J. Han, X. Yan et al., "Infrared small moving target detection using sparse representation-based image decomposition," *Infrared Physics & Technology*, vol. 76, no. 3, pp. 148–156, 2016.

[15] X. Hang, C. L. Zhang, and G. Ruan, "Multimodal detection of a small molecule target using stimuli-responsive liposome triggered by aptamer–enzyme conjugate," *Analytical Chemistry*, vol. 88, no. 3, pp. 1506–1510, 2016.